Materials and Design 49 (2013) 48–57

Contents lists available at SciVerse ScienceDirect

Materials and Design

journal homepage: www.elsevier.com/locate/matdes

Comparative study of fatigue life behaviour of AA6061 and AA7075 alloys under spectrum loadings

K.A. Zakaria, S. Abdullah *, M.J. Ghazali

Department of Mechanical and Materials Engineering, Universiti Kebangsaan Malaysia, 43600 UKM Bangi, Selangor, Malaysia

ARTICLE INFO

Article history:
Received 8 November 2012
Accepted 8 January 2013
Available online 20 January 2013

Keywords:
Aluminium alloys
Elevated temperatures
Fatigue damage
Fatigue life
Load sequence effect

ABSTRACT

The study aimed to present several fatigue tests under loading sequences, and to compare the fatigue life behaviour between AA6061 and AA7075 alloys subjected to spectrum loadings at room and elevated temperatures. Constant amplitude loading (CAL), high-to-low and low-to-high loading sequences were derived from a real-time variable amplitude loading that captured from an engine mount bracket of a 1300 cc automobile under normal driving conditions. The shortest fatigue life was found under CAL, followed by the high-to-low and low-to-high loading sequences at both room and elevated temperatures with difference between the maximum and minimum cycles ranged from 7% to 84%. Increased testing temperature (from 27 °C to 250 °C) exponentially decreased the number of cycles by 75–84%. The effect of loading sequence was more significant at room temperature than at elevated temperature.

1. Introduction

Aluminium alloy is used in many automotive and airplane applications due to light weight, excellent weldability, and corrosion resistance [1]. The use of aluminium alloys in automotive structural application is rapidly growing [2]. In terms of fatigue strength, aluminium alloys still offer lower fatigue strength than high-strength steel [3,4]. On the other hand, as an alternative to steel, aluminium has potentially increasing the efficiency of vehicles by provide a lower weight. The amount of energy needed for transportation decrease with efficiency gains, reducing the emissions, and improving the energy security of the country [5]. In applications, aluminium alloys are used as automotive frames, aircraft structures, wheels, pipelines, etc. The high-temperature parts made of aluminium alloy include the engine block, cylinder head, piston, engine oil pan, intake manifold, and heat exchanger. Generally, the fatigue strength of a material decreases with increased temperature [6–8].

Aluminium alloy grade AA6061 is one of the most widely used alloys in practical applications because of the following properties: good mechanical properties; relative ease with which it can be cast, extruded, rolled, machined, etc.; acceptable in the market; and extensively used for the alloy development [9,10]. Meanwhile, aluminium alloy 7075 is widely used in the aircraft industry since it's provide a high strength and low density alloy [11]. Their combination of high strength with moderate toughness, low density, and high corrosion resistance is required is attractive for a number of aircraft and aerospace structure applications [12–14]. Therefore, according to their applications, both of these aluminium alloys have been studied for many years and enhanced with the aim of increasing the service lifetime. Concurrently, understanding the fatigue behaviour of these alloys can reduce the maintenance costs.

Most engineering components in service are subjected to cyclic loading, and the fatigue fracture is the most common form of failure [15], such as in automobile steering connecting rod, piston connecting rod, marine drive shaft, aircraft body, landing gear. The majority of the fatigue life characterisation of a material is performed under a constant sinusoidal loading [16], which is easier to accommodate with most of the fatigue testing machine's capabilities and also to simplify analysis [17,18]. However, in actual applications, most of the engineering components are subjected to stress amplitude that varies with time [19]. Thus, the failure mechanism associated with variable amplitude loading (VAL) is important to understand to quantify the crack growth rate and fatigue lifetime under the VAL condition [17]. Engineering components operated at elevated temperatures are also vulnerable to fatigue failure at elevated temperatures. Thus, the fatigue life at elevated temperatures must be characterised because some of these components are operated and may fail at elevated temperatures, thereby requiring critical safety levels [20].

The fatigue strength of materials subjected to constant amplitude loading (CAL) at elevated temperature significantly decreases compared with that at room temperature. The fatigue resistance of metals in air decreases with increased temperature. Fatigue at elevated temperatures produces large strain deformation, assists in the crack-initiation process, and accelerates the crack propagation

* Corresponding author. Tel.: +60 3 8911 8411; fax: +60 3 89118389.
E-mail addresses: kamarul1@eng.ukm.my (K.A. Zakaria), shahrum@eng.ukm.my (S. Abdullah), mariyam@eng.ukm.my (M.J. Ghazali).

0261-3069/$ - see front matter © 2013 Elsevier Ltd. All rights reserved.
http://dx.doi.org/10.1016/j.matdes.2013.01.020

rate. Crack initiation occurs much earlier at elevated temperatures. The crack growth rates at elevated temperatures are considerably higher than those at ambient temperatures [7,8,21]. Finally, the total fatigue life decreases with increased temperature. At elevated temperature, the material or structure subjected to cyclic loading may also fail in different modes from normal fatigue fracture [22]. Hence, determining the temperatures at which the strengths of materials become optimal is a critical issue. Many structural components are subjected to cyclic loading at various temperatures; thus, the effects of elevated temperatures on the fatigue life behaviour need to be understood.

The load sequence has been shown to be affected by the material type and loading conditions, such as the magnitude and position of overloads/underloads in the sequence, arrangement of block loadings, stress ratio, mean stress. These parameters affect the fatigue crack initiation and propagation, as well as the total number of cycles to failure [23–32]. However, all these fatigue studies were performed at room temperature. Accordingly, our group was prompted to study the load sequence effect at elevated temperatures.

This paper aimed to investigate the fatigue life of medium- and high-strength aluminium alloys, AA6061 and AA7075, respectively, when subjected to different loading sequences under ambient and heated environments. The fatigue study of these materials at elevated temperatures, particularly under VAL, is important to understand their behaviour and durability for applications at high temperatures. The effect of loading sequences on these alloys at room and elevated temperatures was analysed and compared relative to the three types of loading sequences, i.e., CAL, high-to-low loading, and low-to-high loading sequences. All these loadings were derived from the VALs that were measured on a car component under real-time driving conditions. Fully reversed axial loading fatigue tests were performed using a 100 kN servo-hydraulic fatigue testing machine according to the ASTM: E466-07. The loading sequences and temperatures were expected to affect both aluminium alloys significantly.

2. Theoretical background

Structural or engineering components made of different materials are commonly subjected to cyclic or fluctuating stress in service. Various parts of moving machine are subjected to severe vibration with load fluctuations. The response of a material to cyclic loading significantly differs from that to static loading [33,3]. Fatigue failures occur on a component when subjected to cyclic loadings even though the maximum cyclic load is much lower than the static strength of a material.

There are three major methods can be used to predict the fatigue life, namely, strain-life, stress-life, and fracture mechanics. Strain-life analysis requires a description of the material response to cyclic elastic–plastic strains as well as the relationship between these strains and fatigue life to crack initiation. Strain-life prediction is normally applied with a strain-life model. The strain-life relationship or Coffin–Manson relationship is based on the total strain amplitude [35], which is defined by the following equation:

$$\varepsilon_a = \frac{\sigma'_f}{E}(2N_f)^b + \varepsilon'_f(2N_f)^c \tag{1}$$

where ε_a is the true strain amplitude, σ'_f is the fatigue strength coefficient, b is the fatigue strength exponent, ε'_f is the fatigue ductility coefficient, c is the fatigue ductility exponent, E is the modulus of elasticity, and $2N_f$ is the number of reversals to failure for a particular stress range.

A simple correction was proposed by Morrow [35] and Smith et al. [36], known as the Morrow and Smith–Watson–Topper (SWT) strain-life models, respectively. These two models consider the mean stress effect in the calculation. Morrow's strain-life model is mathematically defined by the following expression:

$$\varepsilon_a = \frac{(\sigma'_f - \sigma_m)}{E}(2N_f)^b + \varepsilon'_f(2N_f)^c \tag{2}$$

and the SWT strain-life model is defined according to the following formula:

$$\varepsilon_a\sigma_{\max} = \frac{(\sigma'_f)^2}{E}(2N_f)^{2b} + \sigma'_f\varepsilon'_f(2N_f)^{b+c} \tag{3}$$

where σ_m is the mean stress and $\sigma_{\max}$ is the maximum stress for the particular cycle.

Among fatigue damage accumulation rules, the linear damage accumulation rule (also known as Palmgren–Miner's rule) is the most commonly used [37]. The fatigue damage accumulation under VAL can be calculated using this rule, which is stated as:

$$D = \sum_{i=1}^{k}\frac{n_i}{N_i} \tag{4}$$

where D is the fatigue damage of the material, n_i is the number of applied loading cycles corresponding to the ith load level, and N_i is the number of cycles to failure at the ith load level from constant amplitude experiments. The calculation of fatigue damage accumulation using Palgren–Miner's rule does not take into account the loading sequence effect [38]. However, the loading sequence effect on the fatigue life was clearly demonstrated in experimental results.

The stress-life (S–N) curve provides useful fatigue data for estimating the number of cycles to failure of material at a certain level of applied stress. The S–N curve for a CAL is plotted on a semi-log or log–log scale that contains few experimental data. The S–N curve was developed by curve fitting on tabular data following the Basquin equation [39], which can be written as:

$$\frac{\sigma}{2} = \sigma_a = \sigma'_f(2N'_f)^b \tag{5}$$

where σ_a is the stress amplitude, σ'_f is the fatigue strength coefficient, $2N'_f$ is the number of reversals, and b is the Basquin exponent.

In term of statistical analysis in engineering practice, the Weibull distribution is a useful theoretical model of life data that has been successfully applied. In this model, a general distribution can be made to model a range of life distributions. From the Weibull analysis, the component's life distributions can be obtained. Representations of the data from graphical plot are useful in detecting outliers, estimating the minimum life, and observing failure times from a Weibull distribution [40]. The two-parameter Weibull distribution function can be written as [41]:

$$F(x;b;c) = 1 - e^{-\left(\frac{x}{b}\right)^c} \tag{6}$$

In term of this study, $F(x; b; c)$ represents the probability of the fatigue life being equal to or less than x, b is a scale parameter, and c is a shape parameter. b and c are estimated by observation.

3. Methodology

Throughout this study, fatigue tests were performed on specimens fabricated from two types of aluminium wrought alloy (AA6061-T6 and AA7075-T6). These materials were received in T6 condition, indicating that the material had been solution heat treated and then artificially aged to increase the alloy strength. This aging process is usually maintained until the maximum or near-maximum strength is achieved [42,43]. The typical chemical compositions [44] of AA6061and AA7075 are shown in Table 1.

The dumbbell-shape specimens were machined from solid wrought bar and their dimensions were set according to the ASTM:

Table 1
Chemical composition of aluminium alloys (wt.%).

Element	Mg	Si	Cu	Mn	F e	Cr	Zn	Ti	Al
AA6061	0.8–1.2	0.4–0.8	0.15–0.40	0.15	0.7	0.04–0.35	0.25	0.15	Bal.
AA7075	2.1–2.9	0.40	1.2–2.0	0.30	0.5	0.18–0.28	5.1–6.1	0.20	Bal.

E466-07. A total of 38 specimens were used for the fatigue tests. As shown in Fig. 1, the specimens were designed with a diameter of 10 mm and gauge length of 30 mm. According to the standard, the length-to-diameter ratio of the specimen is important to ensure that the specimen does not buckle under fully reversed cyclic loading. The specimens were then polished using SiC paper with grit scales of 300, 500, 1000, and 1200 to achieve a mirror-like surface finish and also to prevent stress concentration caused by an irregular surface finish. The experimental process flow is presented in Fig. 2.

To initiate the experimental procedure that comprises a road test for strain data collection and laboratory works, fatigue strain-time histories were measured on an engine mount bracket of a 1300 cc national car (Fig. 3) that was driven onto various road surfaces. An engine mount bracket is one of the automobile components connecting the engine block to vehicle structures. The primary function of the engine mounting system is to support the weight of the engine and ensure that the engine can be freely maintained in its specific design position [45]. The engine mount bracket was directly exposed to static load and unbalanced force (VAL) from the engine. At the same time, the engine mount bracket exposed to the elevated temperature reaching up to 70 °C. The road surface conditions are some of the factors that contribute to VAL under the driving conditions.

This car was driven on a specific road surface, i.e., a residential area road surface (Fig. 4) at an almost constant velocity of 15–25 km/h. This velocity was assumed to be an average speed for most vehicles on such road conditions, and contributes to a stable condition for capturing strain data signals. The residential area road surface was slightly rough with small pit holes and bumps along the road, and was chosen in this study because it inflicted more damage to the engine mount bracket than a normal road surface [46]. The strain gauge of a 2.0 mm gauge length with 120 Ω resistance was fixed on the bracket, and the fixing procedure was based on the ASTM: E1237-93. The gauge size seemed suitable to be fixed within a limited space of the mount bracket. Ensuring that the strain gauge was fixed on a flat surface was important to prevent damage to the strain gauge. The significant strain signals were measured using a fatigue data acquisition system, and the collected data sets were stored in a computer hard disc. Prior to the data collection process, the data acquisition system was calibrated to ensure that the reading of the strain gauge fixed on the bracket remained at almost zero micro-strain before starting the automobile engine. The data acquisition system was able to capture signals up to 100 kHz in frequency. However, the sampling frequency used was 500 Hz to improve data accuracy [47].

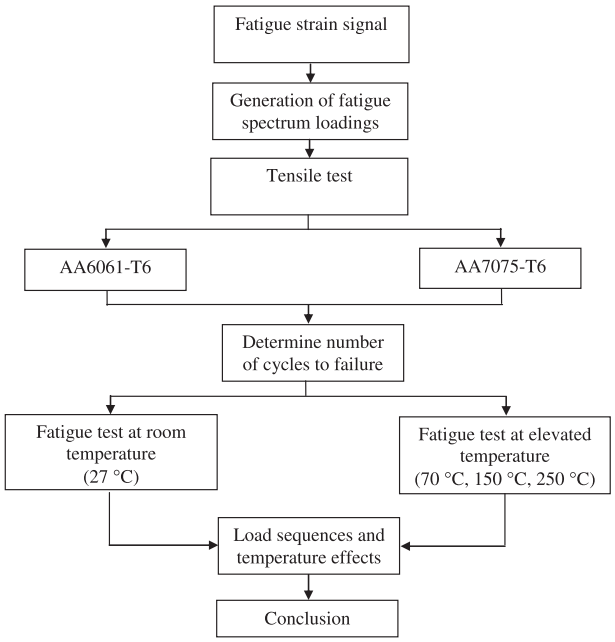

Fig. 2. A flow process of the experimental procedures.

Equivalent damage methods can be used to construct CAL from the service loads. For example, the flight-by-flight load history

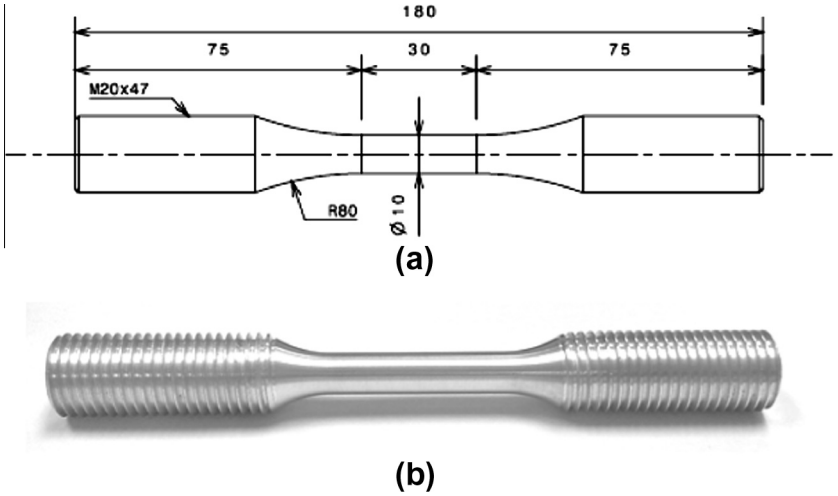

Fig. 1. Specimen design: (a) specimen geometry in millimetres, and (b) image of the actual machined specimen.

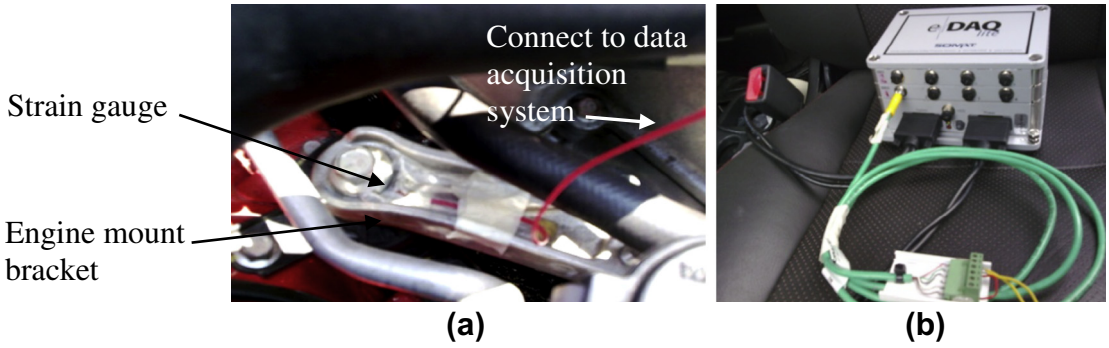

Fig. 3. Capturing time series signal using (a) strain gauge, and (b) fatigue data acquisition system SoMat eDAQ.

Fig. 4. Surface condition of the residential area road.

(random loading) can be converted into CAL based on the equivalent damage [48]. Pereira et al. [49] used the maximum stress that induces the same damage when applied at the same total number of cycles of block loading. For automotive application, Abdullah et al. [50] found good justification for the retention of fatigue damage features while performing fatigue data editing for accelerated fatigue tests. This finding has prompted authors to assume or hypothesize the concept of retaining the total fatigue damage for constructing the CAL, high-to-low loading, and low-to-high loading sequences. The damage produced by these three loading sequences is designed to be similar or equivalent to the damage produced by the VAL original time series, as shown in a typical example in Fig. 5.

The damage values were calculated using the Coffin–Manson (CM) strain-life relationship because the load sequence time histories were designed at zero mean stress. Each load case consisted of four block loading cycles arranged under CAL, high-to-low loading, and low-to-high sequences. The total number of cyclic load decreased from about 3650 cycles in the random nature of the original signals to 40 cycles in each case of designed load sequence to reduce the laboratory testing time or to accelerate fatigue testing.

The loading sequence of the strain signal was then converted into stress using the Ramberg–Osgood equation, which is stated as:

$$\varepsilon = \frac{\sigma}{E} + \left(\frac{\sigma}{K}\right)^{\frac{1}{n}} \tag{7}$$

where ε is the strain amplitude in the cycles, σ is the stress amplitude, E is the modulus of elasticity of material, K is the strain hardening coefficient, and n is the strain hardening exponent. A "goal-seeking" approach was used based on a programming language that solves the iteration process of this equation. The flowchart of this programming step is presented in Fig. 6. The designed spectrum loading sequences, as shown in Fig. 7, were amplified to about 50% of the ultimate strength of material to accelerate the fatigue tests.

For the next stage, tensile tests were performed to determine the mechanical properties of the as-received material for both aluminium alloy types. The test was performed using a 100 kN universal testing machine according to the ASTM: E8M-11. The test

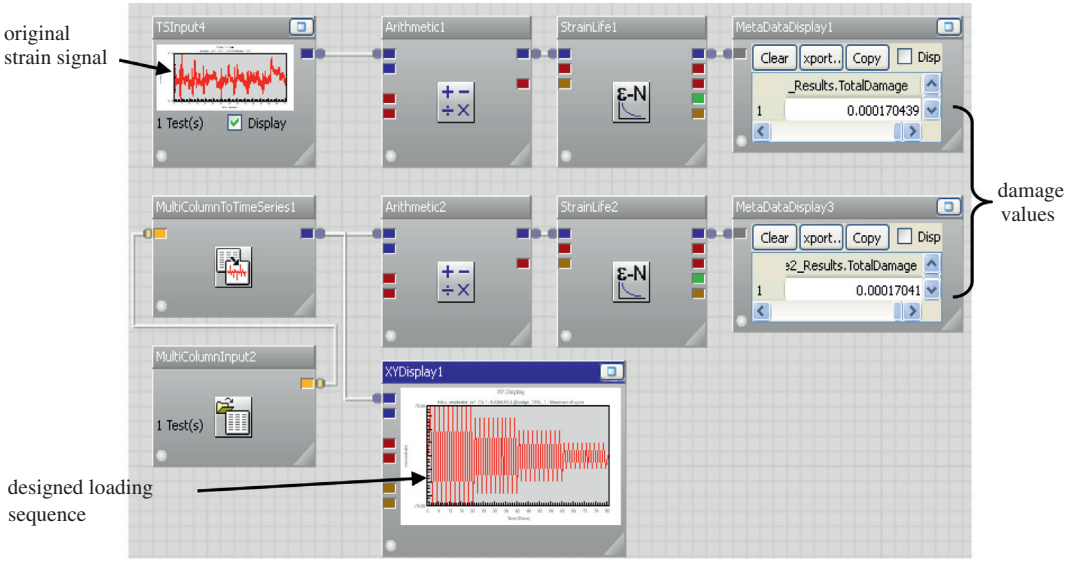

Fig. 5. Loading sequence designed by retaining the damage value.

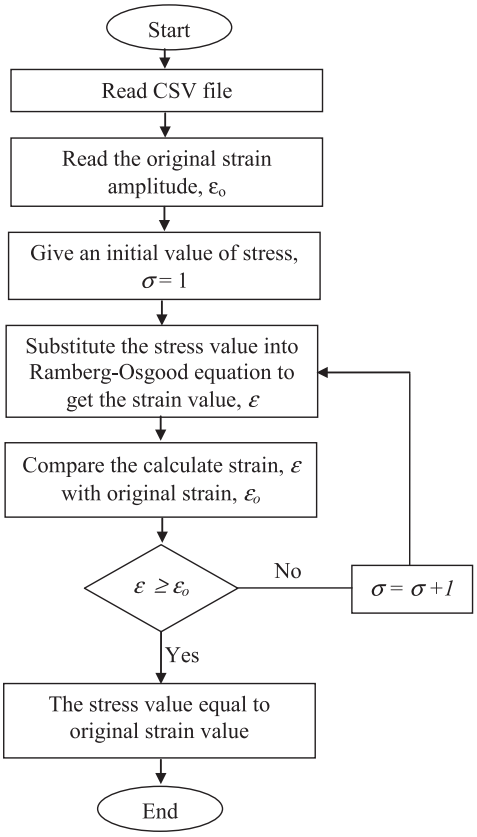

Fig. 6. Flowchart of conversion strain to stress.

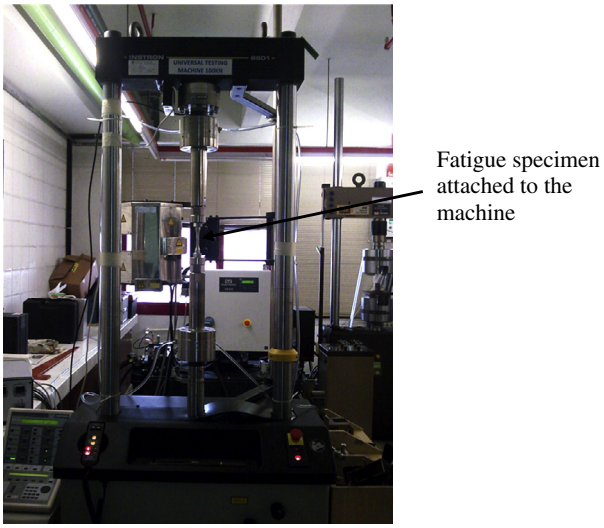

Fig. 8. Servo-hydraulic fatigue testing machine (100 kN).

was conducted using a cross-head speed of 1.5 mm/min accommodated for 25 mm gauge length of the extensometer. Fatigue tests were finally carried out using different loading sequences at room and elevated temperatures. Accordingly, the fatigue life behaviour was observed and analysed. The cyclic tests were performed following the ASTM: E466-07. The tests were conducted under the load-controlled mode using fully reversed axial loading with a stress ratio $R = -1$. The cyclic load was a sinusoidal signal operated at 5 Hz. This testing frequency was based on the fatigue test at elevated temperatures performed by Juijerm et al. [8]. The fatigue tests were conducted at ambient (27 °C) and elevated (70, 150, and 250 °C) temperatures. This elevated temperature regime was chosen based on the maximum temperature of the engine mount bracket and cylinder head, where a peak temperature as high as 250 °C was reached during service [6]. The configuration of the specimen setting in the fatigue testing machine is shown in Fig. 8.

4. Results and discussion

The recorded strain signal time history is presented in Fig. 9. The time history plot of the captured signal shows that the signal has a total of 3650 cycles based on rainflow cycles, which gave the maximum value of 97.53 με, the minimum value of 94.26 με, and the mean value of 4.55 με. The strain-life of the original signals was analysed to calculate the fatigue damage based on the CM, Morrow, and SWT strain-life models. The summary of the original strain signal parameter and its damage values are shown in Table 2. Results showed that the damage values did not differ much among these three models, with a difference percentage of less than 1%, because the captured strain signal had almost zero mean values. Therefore, no significant difference was observed among the calculated damage values using the different strain-life models. The SWT strain-life model reportedly produces more conservative life estimates for the tensile mean stress, and the Morrow strain-life model is preferred for compressive mean stress [34].

A typical example of a three-dimensional cycle histogram and the corresponding damage histogram on AA6061 are shown in Fig. 10a and b, respectively. Both plots showed the result of a rainflow cycle count for the critical location of an engine mount bracket. These histograms gave an idea on the source of the majority of the damage. Numerous cycles originated from the low-strain range and few cycles were from the high-strain range. The number of cycles at that particular strain range and mean represented by the height of each tower. Results showed that the high-strain ranges inflicted most of the damage.

Tensile tests were performed to provide information on the mechanical properties in terms of the strength and ductility of the materials under uniaxial loading. These properties were useful for determining the characteristics of materials, alloy development, and design under certain circumstances. Fig. 11 shows the typical stress–strain curve for the as-received material for both alloys. The tensile test results in the ambient-temperature regime revealed that AA7075 had higher ultimate strength and modulus elasticity than AA6061 alloy. The ultimate strength of AA7075

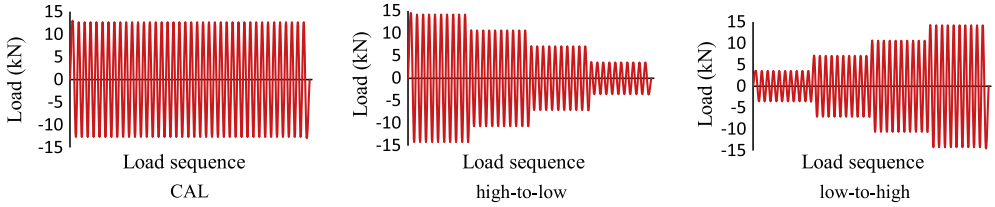

Fig. 7. Typical loading sequences used for fatigue tests.

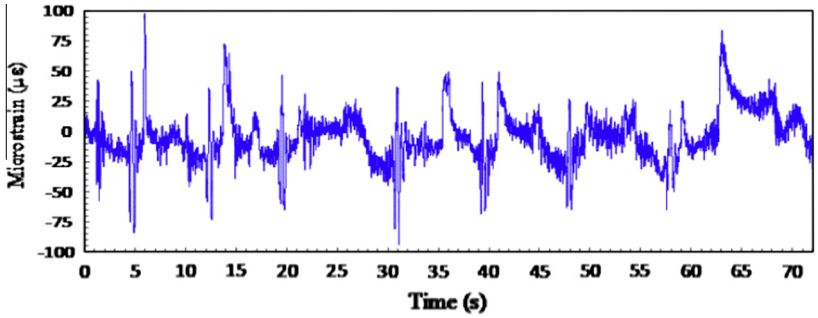

Fig. 9. A real-time strain signal collected on the residential area road surface.

Table 2
Original strain signal parameters.

Number of cycles	Max (με)	Min (με)	Mean (με)	Range (με)	Total damage ($\times 10^{-7}$ block cycles)		
					CM	Morrow	SWT
3650	97.53	−94.26	−4.55	191.79	1.70	1.69	1069

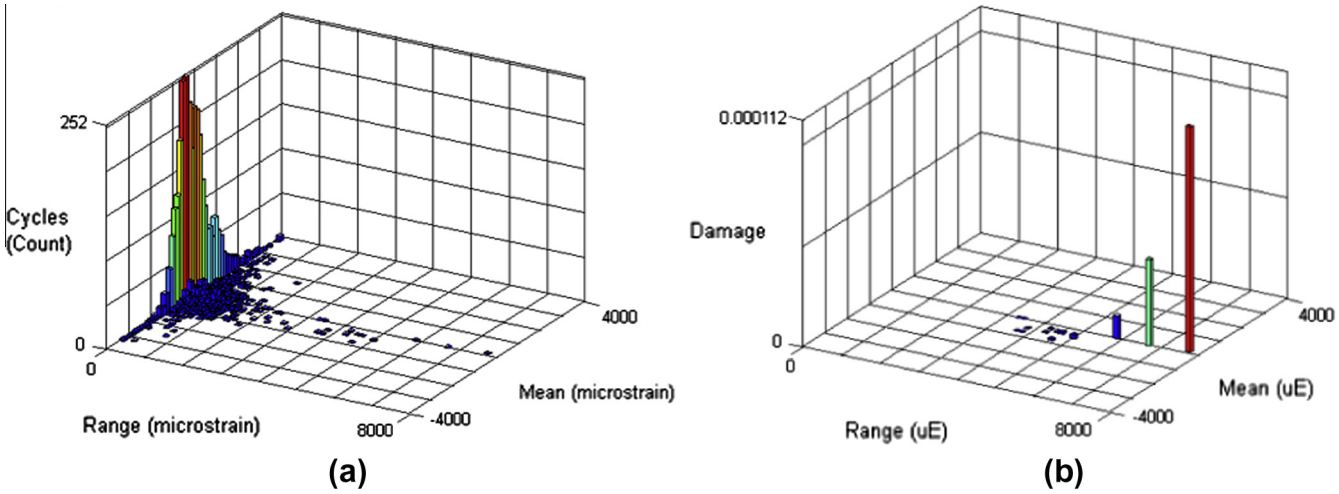

Fig. 10. Typical example of a (a) fatigue cycle histogram and (b) fatigue damage histogram calculated based on the CM model.

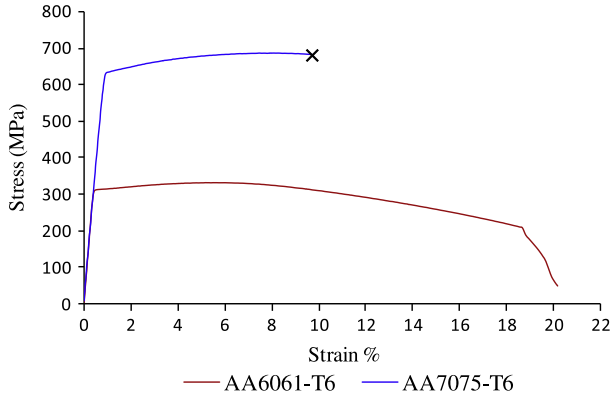

Fig. 11. Typical stress–strain curve of AA6061 and AA7075.

was found to be 687 MPa, and its modulus of elasticity was calculated as 72.4 GPa. Meanwhile, the ultimate strength of AA6061 was 332 MPa and its modulus of elasticity was 70.1 GPa. Hence, the as-received AA7075 had better properties compared than AA6061. Theoretically, AA6061 belongs to the category of medium-strength aluminium alloy [51]. This classification is based on the presence of Zn, Cu and Mg in AA7075, which significantly contribute to precipitation hardening. The microstructure of AA7075 is also highly heterogeneous under peak-hardened conditions [52].

As the basic guideline for fatigue life analysis, the *S–N* curve for CAL was plotted on a semi-log or log–log scale that contained few experimental data. Fig. 12 shows a semi-log plot of stress amplitude versus the number of cycles to failure at room temperature for both aluminium alloys. This *S–N* curve showed a general trend of increased fatigue life with decreased cyclic stress amplitude, which is normally observed in other aluminium alloys. The *S–N* curves of as-received AA6061 and AA7075 were obtained from the experimental data, and two equations that represented their *S–N* curves can be defined by Eqs. (8) and (9), respectively:

$$\sigma_{a(6061)} = 651(N_f)^{-0.12} \tag{8}$$

$$\sigma_{a(7075)} = 1253(N_f)^{-0.13} \tag{9}$$

where σ_a is the stress amplitude and N_f is the number of cycles to failure. Notably, AA7075 alloy had a longer fatigue life than AA6061 at each stress level. The curve fitting revealed that the fatigue strength coefficient and Basquin exponent for AA6061 were

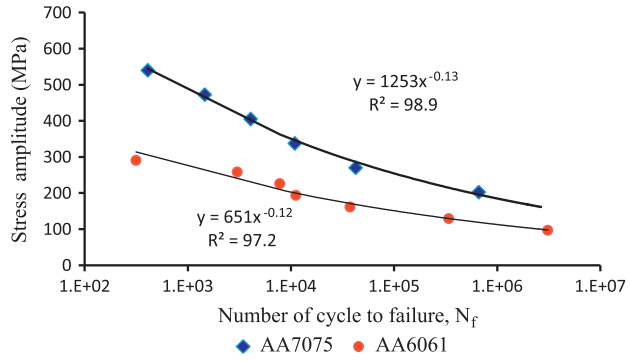

Fig. 12. Comparison of the *S–N* curves of AA6061 and AA7075.

651 MPa and −0.12, respectively, with a regression value R^2 of 97.2%. On the other hand, the fatigue strength coefficient and the Basquin exponent for AA7075 were 1253 MPa and −0.12, respectively, with R^2 = 98.8%. The obtained regression values indicated that the tabular data well fitted both plotted curves. The longer fatigue lives of the AA7075 specimens were mainly attributed to their higher strength.

A comparison of the fatigue lives of AA6061 and AA7075 under different loading sequences at room temperature is presented in Fig. 13. The number of cycles to failure was the highest under the low-to-high loading sequence, followed by the high-to-low sequence and CAL for both aluminium alloys. For AA6061, the number of cycles under low-to-high loading sequence was 56% higher than that under CAL. For AA7075, the difference between these loading sequences was 84%. This difference can be attributed to the different properties of these two alloys, which indicated that AA7075 was more strongly affected by the loading sequences than AA6061. The load interactions that existed under VAL resulted in a longer fatigue lives than under CAL. The number of cycle to failure for both types of aluminium alloy was also higher for low-to-high than high-to-low loading sequences. According to Walter et al. [53], the material initially showed strong softening followed by continuous linear softening up to the initiation of a macro-crack, which was observed in the single-step experiments. Consequently, the softening potential increased with increased total stress or strain amplitude; thus, the lifetimes decreased because of higher stress and plastic deformation during one cycle. By contrast, low initial loads resulted in longer normalised lifetimes.

The effect of elevated temperatures for each type of loading sequence on the fatigue life is exhibited in Fig. 14a and b. The number of cycle to failures for both alloys notably decreased exponentially with increased temperature. A relationship between the number of cycles to failure N_f, and testing temperature T, can be obtained from the curve fitting equation. For aluminium alloy, the AA6061 curve-fitting equation for CAL can be defined as:

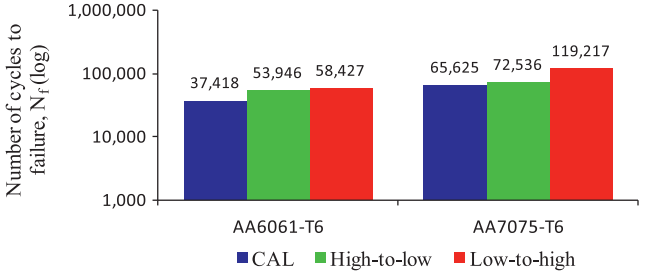

Fig. 13. Comparison of fatigue lives under different loading sequences of AA6061 and AA7075 performed at room temperature.

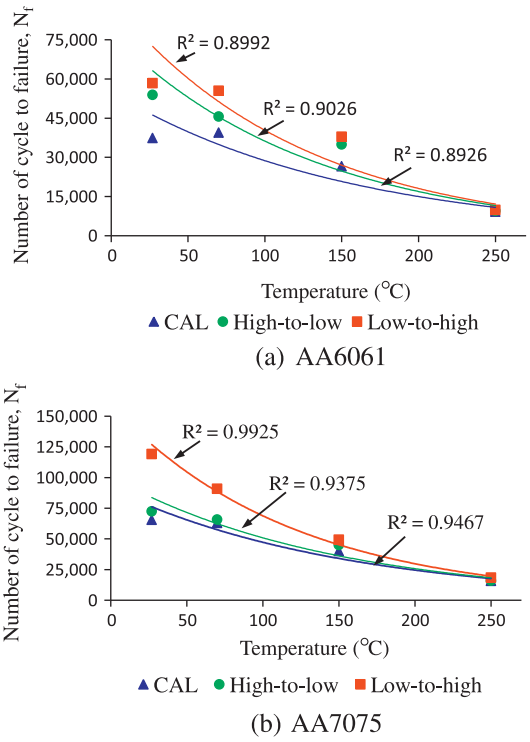

Fig. 14. Comparison of the numbers of cycles to failure under the different loading sequences for both alloys.

$$N_{f(CAL)} = 55079e^{-0.007T} \quad (10)$$

The equations for high-to-low and low-to-high loading sequences were defined by Eqs. (11) and (12), respectively:

$$N_{f(HL)} = 77570e^{-0.008T} \quad (11)$$

$$N_{f(LH)} = 90016e^{-0.008T} \quad (12)$$

For AA7075, the curve-fitting equation for each loading sequences was represented by Eqs. (13)–(15):

$$N_{f(CAL)} = 90840e^{-0.007T} \quad (13)$$

$$N_{f(HL)} = 100519e^{-0.007T} \quad (14)$$

$$N_{f(LH)} = 159014e^{-0.008T} \quad (15)$$

The R^2 value of more than 89% indicated that the tabular data well fitted the plotted curves. The trends of plotted curves are agreed with the findings of Hong et al. [54]. With increased temperature, the fatigue lives decreased because of both the exterior aggressive conditions and change in internal parameters of the material itself. Increased testing temperature can accelerate the rate of oxidation and induce the irreversibility of cyclic slip, thereby inflicting damage to the microstructure [39]. The results of tensile tests performed at elevated temperatures indicated considerable degradation of strength with increased temperature [7]. All these changes affected the fatigue lives of materials.

Fig. 15 shows that the box plot of the total fatigue life ranged between the low-to-high sequence and CAL for each tested temperature. The highest difference between the number of cycles to failure under these two loading sequences was found to be at 27 °C, whereas the smallest difference was at 250 °C. For AA6061, the number of cycles to failure under low-to-high loading sequence was 56% higher than that under CAL at 27 °C, compared with only 7% at 250 °C. For AA7075, the number of cycles to failure

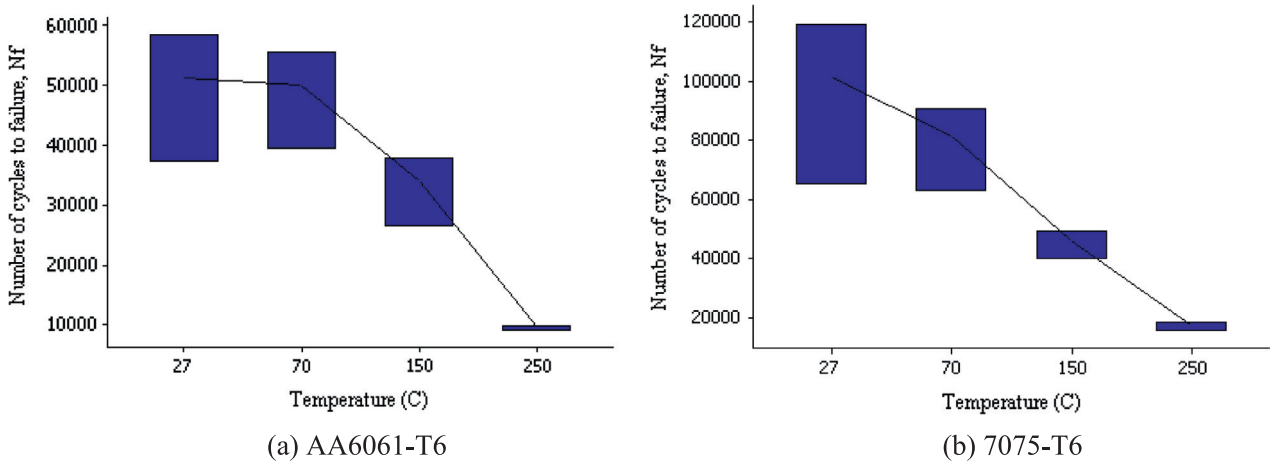

Fig. 15. Total fatigue life range for all cases of loading sequences tested at different operating environment temperatures.

under low-to-high loading sequence was 82% higher than that under CAL at 27 °C, compared with only 17% at 250 °C. These results clearly indicated that the loading sequence effect was more conserved at ambient temperature (27 °C) than at 250 °C. These experimental findings were in accordance with the previous study and are supported with the statement given by previous works [7,8,55,56].

At the room-temperature regime, plastic deformation tended to be higher under VAL, which intensified the crack closure effect and consequently reduced the fatigue crack propagation rate compared with CAL [55]. At the same time, increased temperature increased the plastic deformation of the aluminium alloys [8,56]. The tensile test performed at elevated temperature also showed that the modulus of elasticity of the material decreased with increased temperature [7]. As a result, the effect of plastic deformation under VAL relative to the temperature increase was reduced. Therefore, the loading sequence effect was more significant at room temperature than at elevated temperatures.

The fatigue life of structures or components is a function of many variables, including the loading conditions, geometry, material behaviour, and environmental conditions, which produce scattered results [57]. This problem leads to the necessity of performing statistical analyses during designing and manufacturing for the safe utilisation of materials. One of these analyses is the Weibull distribution, which can model the experimental data of different parameters [41]. The two parameters of the Weibull distribution are the scale and shape parameters, which show the characteristic and slope of the Weibull distribution plot, respectively. These parameters, as determined using a statistics-based software package, were 7.322 (shape factor) and 53,601 (scale factor) for AA6061, as well as 3.867 (shape factor) and 94,982 (scale factor) for AA7075, respectively. The lower shape factor for AA7075 showed that the fatigue life was more scattered when subjected to different loading sequences. In other words, the load sequence significantly affected the fatigue life.

The cumulative distribution failure (CDF) plots the value of each observation against the percentage of values in the samples that are less than or equal to that value [41]. In this study, the CDF was used to determine the percentage of specimen failure in the test after a certain number of cycles. The CDF plots of the number of cycles to failure for AA6061 and AA7075 when subjected to sequence loadings are shown in Fig. 16a and b, respectively. The empirical CDF plot data showed normal distribution with a mean of 49,930 cycles for AA6061 and 85,793 cycles for AA7075. When a percentile line was inserted at 60,000 cycles of the applied load, about 80% of AA6061 samples failed below this value. Meanwhile,

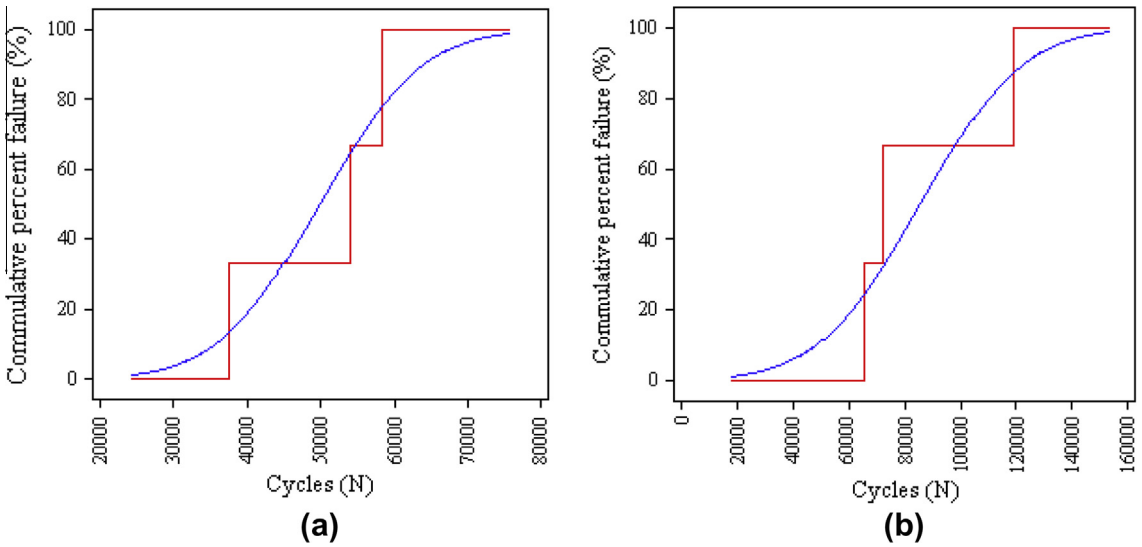

Fig. 16. Empirical CDF plots for (a) AA6061 and (b) AA7075, subjected to all loading cases at room temperature.

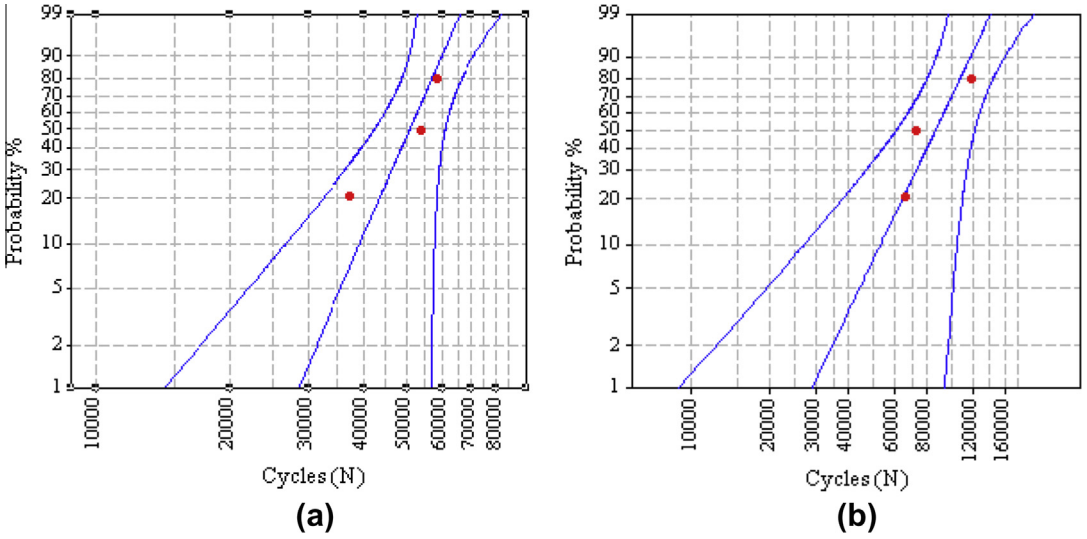

Fig. 17. Probability plot of (a) AA6061 and (b) AA707.5, subjected to all loading cases at room temperature.

only about 20% of AA7075 samples failed under the same cycle loading. Therefore, the higher accumulated failure percentage in AA6061 than AA7075 indicated that AA6061 had a lower fatigue life.

The Weibull cumulative probability plot at 95% confidence interval of the numbers of cycles to failure for AA6061 and AA7075 are shown in Fig. 17a and b, respectively. The number of cycles to failure at a certain probability percentage, which was subjected to loading sequence, can be determined from the plot. For example, a 90% probability of failure for AA6061 occurred between 50,000 and 70,000 cycles. On the other hand, a 90% probability of failure for AA7075 occurred between 115,000 and 160,000 cycles. For probability analysis, at least three data were required. In this study, three data points were used based on the CAL, high-to-low loading, and low-to-high loading sequences. The probability results for 95% confidence intervals caused about 5% error at 90% probability [57]. Thus, the results were considered acceptable.

5. Conclusion

The concept of retaining damage values was used to derive the loading sequences from the real-time experimental measured time histories of a car component that exhibited the VAL pattern. This approach was important in initiating and developing the loading sequences throughout this research. Fatigue life assessment showed that the number of cycles to failure for both types of aluminium alloys, AA6061 and AA7075, were significantly affected by the loading sequences. The total fatigue lives were the shortest under the CAL, followed by the high-to-low and low-to-high loading sequences for both room and elevated temperatures. The differences among the total cycles ranged from 7% to 84%. The total fatigue life also exponentially decreased from 75% to 84% with increased temperature. Therefore, the loading sequence effects must be considered in the fatigue life assessment of structures and components.

The loading sequence effects were found to decrease with increased temperature. At 27 °C, the number of cycles to failure under low-to-high loading sequence was found to be 56% and 84% longer than under CAL for both alloys, respectively. However, at 250 °C, the number of cycles to failure under low-to-high loading sequence was only 7% longer for AA6061 and 17% longer for AA7075 compared with constant loading. Overall, the experimentally determined fatigue lives at both room and elevated temperatures were observed to depend on the loading sequences as well as on the interaction of multiple overloads and underloads that have been found in the VAL.

Apart from this conventional analysis, a statistical-based procedure was also carried out as part of the validation process. Thus, the Weibull distribution was used to offer an alternative approach to the prediction of the probability percentage of failure for both aluminium alloys subjected to different loading sequences. AA7075 showed a higher tensile strength and better fatigue life behaviour than AA6061. Considering the three loading sequences used, the probability plot indicated that 50% of data failed below 90,000 and 50,000 cycles for AA7075 and A6061, respectively.

References

[1] Feng MD, Qiu HG, Fei HZ, Yu ZZ, Shu CC, Hua ZW. Crack initiation and propagation of cast A356 aluminium alloy under multi-axial cyclic loadings. Int J Fatigue 2008;30:1843–50.
[2] Zhu X, Shyam A, Ones JWJ, Mayer H, Lasecki JV, Allison JE. Effects of microstructure and temperature on fatigue behaviour of E319-T7 cast aluminium alloy in very long life cycles. Int J Fatigue 2006;28:1566–71.
[3] Murthy VSR, Jena AK, Gupta KP. Structure and properties of engineering materials. New Delhi: Tata McGraw-Hill Publishing Company Limited; 2003.
[4] Campbell FC. In: Elements of metallurgy and engineering alloys. Metal Park (OH): ASM International; 2008.
[5] Hadley SW, Das S, Miller JW. Aluminium R&D for automotive uses and the department of energy's role. A report: prepared for the office of advanced automotive technologies, office of transportation technologies and U.S. department of energy. Washington (DC); 2000.
[6] Zhu X, Shyam A, Jones JW, Mayer H, Lasecki JV, Allison JE. Effects of microstructure and temperature on fatigue behaviour of E319-T7 cast aluminium alloy in very long life cycles. Int J Fatigue 2006;28:1566–71.
[7] Uematsu Y, Akita M, Nakajima M, Tokaji K. Effect of temperature on high cycle fatigue behaviour in 18Cr–2Mo ferritic stainless steel. Int J Fatigue 2008;30:642–8.
[8] Juijerm P, Altenberger I. Effect of temperature on cyclic deformation behaviour and residual stress relaxation of deep rolled under-aged aluminium alloy AA6110. Mater Sci Eng A 2007;452–453:475–82.
[9] Jogi BF, Brahmankar PK, Nandar VS, Prasad PC. Some studies on fatigue crack growth rate of aluminium alloy 6061. J Mater Process Technol 2008;201:380–4.
[10] Ozturk F, Sisman A, Toros S, Kilic S, Picu RC. Influence of aging treatment on mechanical properties of 6061 aluminium alloy. Mater Des 2010;31:972–5.
[11] Zhao Z, Frankel GS. On the first breakdown in AA7075-T6. Corros Sci 2007;49:3064–88.
[12] Rafi HK, Ram GDJ, Phanikumar G, Rao KP. Microstructure and tensile properties of friction welded aluminium alloy AA7075-T6. Mater Des 2010;31:2375–80.
[13] Oskoiei RH, Ibrahim RN. The effect of typical flight temperatures on the fatigue behaviour of Al 7075-T6 clamped plates. Mater Sci Eng A 2011;528:1527–33.
[14] Lee WS, Sue WC, Lin CF, Wu CJ. The strain rate and temperature dependence of the dynamic impact properties of 7075 aluminium alloy. J Mater Process Technol 2000;100:116–22.

[15] Zhao T, Zhang J, Jiang Y. A study of fatigue crack growth of 7075-T651 aluminium alloy. Int J Fatigue 2008;30:1169–80.
[16] Post NL, Case SW, Lesko JJ. Modelling the variable amplitude fatigue of composite materials. Int J Fatigue 2008;30:2064–86.
[17] Wei LW, de los Rios ER, James MN. Experimental study and modelling of short fatigue crack growth in aluminium alloy A17010-T7451 under random loading. Int J Fatigue 2002;24:963–75.
[18] Beden SM, Abdullah S, Ariffin AK, Al-Asady NA, Rahman MM. Fatigue life assessment of different steel based shell materials under variable amplitude loading. Eur J Sci Res 2009;29:157–69.
[19] Zhang YH, Maddox SJ. Investigation of fatigue damage to welded joints under variable amplitude loading spectra. Int J Fatigue 2009;31:138–52.
[20] Pulido J. Reliability analysis for components under thermal mechanical loadings. in: Proceedings of annual reliability and maintainability symposium, art. no. 60175449; 2012.
[21] Tokaji. High cycle fatigue behaviour of Ti–6Al–4V alloy at elevated temperatures. Scripta Mater. 2006;54:2143–8.
[22] Bahaideen FB, Saleem AM, Hussain K, Ripin ZM, Ahmad ZA, Samad Z, et al. Modern Appl Sci 2009;3:52–61.
[23] Lu Z, Liu Y. Experimental investigation of random loading sequence effect on fatigue crack growth. Mater Des 2011;32:4773–85.
[24] Lee EU, Glinka G, Vasudevan AK, Iyyer N, Phan ND. Fatigue of 7075-T651 aluminium alloy under constant and variable amplitude. Int J Fatigue 2009;31:1858–64.
[25] Tao JX, Smith S, Duff A. The effect of overloading sequences on landing gear fatigue damage. Int J Fatigue 2009;31:1837–47.
[26] Borego LP, Ferreira JM, Costa JM. Partial crack closure under block loading. Int J Fatigue 2008;30:1787–96.
[27] Beden SM, Abdullah S, Ariffin AK, Al-Asady NA. Fatigue crack growth simulation of aluminium alloy under spectrum loading. Mater Des 2010;31:3449–56.
[28] Ray A, Patankar R. Fatigue crack growth under variable-amplitude loading: Part I. Model formulation in-state space setting. Appl Math Modell 2001;2001(25):979–94.
[29] Schijve J, Skorupa M, Skorupa A, Machniewicz T, Grusczynski P. Fatigue crack growth in the aluminium alloy D16 under constant and variable amplitude loading. Int J Fatigue 2004;2004(26):1–15.
[30] Borrego LP, Costa JM, Ferreira JM. Fatigue crack growth in thin aluminium alloy sheet under loading sequences with periodic overloads. Thin-Walled Struct 2005;43:772–88.
[31] Zitounis V, Irving PE. Fatigue crack acceleration effects during tensile underloads in 7010 and 8090 aluminium alloys. Int J Fatigue 2007;29:108–18.
[32] Mikheevskiy S, Glinka G. Elastic–plastic fatigue crack growth analysis under variable amplitude loading spectra. Int J Fatigue 2009;31:1828–36.
[33] Varvani-Farahani A, Kianoush MR, Sharma M. Fatigue failure assessment of engineering components under service loading conditions. Mater Des 2007;28:575–80.
[34] Draper J. Modern metal fatigue analysis. United Kingdom: Emas Publishing; 2007.
[35] Morrow J. Fatigue design handbook, advances in engineering. Warrendale (PA): Society of Automotive Engineers; 1968.
[36] Smith KN, Watson P, Topper TH. A stress–strain function for the fatigue of metals. J Mater 1970;4:767–78.
[37] Liu Y, Mahadevan S. Stochastic fatigue damage modeling under variable amplitude loading. Int J Fatigue 2007;2007(29):1149–61.
[38] Ngiau C, Kujawski D. Sequence effects of small amplitude cycles on fatigue crack initiation and propagation in 2024-T351 aluminium. Int J Fatigue 2001;23:807–15.
[39] Liu Y, Yu JJ, Xu Y, Sun XF, Guan HR, Hu GQ. High cycle fatigue behaviour of a single crystal super alloy at elevated temperatures. Mater Sci Eng A 2007;454–455:357–66.
[40] Lee YL, Pan J, Hathaway RB, Barkey ME. Fatigue testing and analysis (theory and practice). USA: Elsevier Butterworth-Heinemann; 2005.
[41] Sivapragash M, Lakshminarayanan PR, Karthikeyen R, Raghukandan K, Hanumantha M. Fatigue life prediction of ZE41A magnesium alloy using Weibull distribution. Mater Des 2008;29:1549–53.
[42] Adesola AO, Odeshi AG, Lanke UD. The effects of aging treatment and strain rates on damage evolution in AA6061 aluminium alloy in compression. Mater Des 2013;45:212–21.
[43] Philip A, Schweitzer PE. Metallic material. New York: Marcel Dekker, Inc.; 2003.
[44] Boyer HE, Gall TL. In: Metal handbook, desk edition. Metal Park (OH): American Society for Metal; 1985.
[45] Yu Y, Naganathan NG, Dukkipati RV. A literature review of automotive vehicle engine mounting systems. Mech Machine Theory 2001;36:123–42.
[46] Zakaria KA, Abdullah S, Ghazali MJ, Nuawi MZ, Padzi MM. Fatigue damage assessment of the engine mount bracket using a statistical based approach. Adv Mater Res 2011;197–198:1631–5.
[47] Al-Asady NA, Abdullah S, Ariffin AK, Beden SM, Rahman MM. Comparison between experimental road data and finite element analysis data for automotive lower suspension arm. Eur J Sci Res 2009;29:557–71.
[48] Robert M, Engle JR. Damage accumulation techniques in damage tolerance analysis. In: Chang, Rudd, editors. Damage tolerance in metallic structures. Ann Arbor: American Society for Testing and Material; 1984.
[49] Pereira HFSG, de Jesus AMP, Ribeiro AS, Fernandas AA. Influences of loading sequence and stress ratio on fatigue damage accumulation of a structural component. Sci Technol Mater 2008;20:60–7.
[50] Abdullah S, Choi JC, Giacomin JR, Yates JR. Bump extraction algorithm for variable amplitude fatigue loading. Int J Fatigue 2006;28:675–91.
[51] Demir H, Gunduz S. The effects of aging on machinability of 6061 aluminium alloy. Mater Des 2009;30:1480–3.
[52] Zhao T, Zhang J, Jiang Y. A study of fatigue crack growth of 7075-T651 aluminium alloy. Int J Fatigue 2008;30:1169–80.
[53] Walter M, Aktaa J, Lerch M. Failure behaviour of EUROFER 97 in the low cycle fatigue region under multi-step loading. Int J Fatigue 2008;30:568–73.
[54] Hong SG, Lee SB. Mechanism of dynamic strain aging and characterization of its effect on the low-cycle fatigue behaviour in type 316L stainless steel. J Nucl Mater 2005;340:307–14.
[55] Yamada K, Cao Q, Okado N. Fatigue crack growth measurements under spectrum loading. Eng Fract Mech 2000;66:483–97.
[56] Srivatsan TS, Siram S, Daniels C. Influence of temperature on cyclic stress response and fracture behaviour of aluminium alloy 6061. Eng Fract Mech 1997;56(4):531–50.
[57] Gope PC. Determination of sample size for estimation of fatigue life by using Weibull or log-normal distribution. Int J Fatigue 1999;21:745–52.